



Platform



Patient



Machine

# SunCHECK™

## One Database for Complete Quality Management

[Learn more >](#)



- Plan Quality Checks
- Secondary Dose Calculations
- Pre-Treatment QA
- In-Vivo Monitoring



- Standardized Routine QA
- Direct Device Control
- Automated Imaging, MLC & VMAT QA
- Protocol-Based QA

# Physiologically personalized coronary blood flow model to improve the estimation of noninvasive fractional flow reserve

Xiujian Liu<sup>1</sup> | Chuangye Xu<sup>2</sup> | Simin Rao<sup>3</sup> | Ye Zhang<sup>3</sup> | Dhanjoo Ghista<sup>4</sup> |  
 Zhifan Gao<sup>1</sup> | Guang Yang<sup>5,6</sup>

<sup>1</sup> School of Biomedical Engineering, Sun Yat-sen University, Shenzhen, China

<sup>2</sup> School of Medicine, Southern University of Science and Technology, Shenzhen, China

<sup>3</sup> Beijing GuanShengYun Medical Technology Co.,Ltd, Beijing, China

<sup>4</sup> University 2020 Foundation, Northborough, Massachusetts, USA

<sup>5</sup> National Heart and Lung Institute, Imperial College London, London, UK

<sup>6</sup> Cardiovascular Research Centre, Royal Brompton Hospital, London, UK

## Correspondence

Zhifan Gao, School of Biomedical Engineering, Sun Yat-sen University, Shenzhen, 518107, China.  
 Email: gaozhifan@mail.sysu.edu.cn

## Funding information

the Key-Area Research and Development Program of Guangdong Province, Grant/Award Number: 2019B010110001; the National Natural Science Foundation of China, Grant/Award Numbers: 62101610, 62101606; the China Postdoctoral Science Foundation, Grant/Award Number: 2021M693673; the Shenzhen Science and Technology Program, Grant/Award Number: 2021A14; the British Heart Foundation, Grant/Award Numbers: TG/18/5/34111, PG/16/78/32402; the European Research Council Innovative Medicines Initiative, Grant/Award Numbers: DRAGON, H2020-JT-IMI2 101005122; the AI for Health Imaging Award, Grant/Award Numbers: CHAMELEON, H2020-SC1-FA-DTS-2019-1 952172; the UK Research and Innovation Future Leaders Fellowship, Grant/Award Number: MR/V023799/1

## Abstract

**Purpose:** Coronary outlet resistance is influenced by the quantification and distribution of resting coronary blood flow. It is crucial for a more physiologically accurate estimation of fractional flow reserve (FFR) derived from computed tomography angiography (CTA), referred to as FFRCT. This study presents a physiologically personalized (PP)-based coronary blood flow model involving the outlet boundary condition (BC) and a standardized outlet truncation strategy to estimate the outlet resistance and FFRCT.

**Methods:** In this study, a total of 274 vessels were retrospectively collected from 221 patients who underwent coronary CTA and invasive FFR within 14 days. For FFRCT determination, we have employed a PP-based outlet BC model involving personalized physiological parameters and left ventricular mass (LVM) to quantify resting coronary blood flow. We evaluated the improvement achieved in the diagnostic performance of FFRCT by using the PP-based outlet BC model relative to the LVM-based model, with respect to the invasive FFR. Additionally, in order to evaluate the impact of the outlet truncation strategy on FFRCT, 68 vessels were randomly selected and analyzed independently by two operators, by using two different outlet truncation strategies at 1-month intervals.

**Results:** The per-vessel diagnostic performance of the PP-based outlet BC model was improved, based on invasive FFR as reference, compared to the LVM-based model: (i) accuracy/sensitivity/specificity: 91.2%/90.4%/91.8% versus 86.5%/84.6%/87.6%, for the entire dataset of 274 vessels, (ii) accuracy/sensitivity/specificity: 88.7%/82.4%/90.4% versus 82.4%/76.5%/84.0%, for moderately stenosis lesions. The standardized outlet truncation strategy showed good repeatability with the Kappa coefficient of 0.908.

**Conclusions:** It has been shown that our PP-based outlet BC model and standardized outlet truncation strategy can improve the diagnostic performance and repeatability of FFRCT.

## KEYWORDS

computational fluid dynamics, coronary blood flow model, coronary computed tomography angiography, fractional flow reserve, outlet boundary conditions

## 1 | INTRODUCTION

Fractional flow reserve (FFR) derived from computed tomography angiography (CTA), called FFRCT, has been recognized as a useful technique to assess the

hemodynamic significance of coronary stenosis.<sup>1,2</sup> With the employment of computational fluid dynamics (CFD), FFRCT has expanded the diagnostic capabilities of coronary CTA, and has the potential to serve as a gatekeeper for invasive coronary angiography (ICA).<sup>3,4</sup>

As with the definition of invasive FFR, FFRCT refers to the ratio of mean distal coronary pressure to the pressure at the coronary artery ostium during maximum hyperemia. Thus, the value of FFRCT is determined directly by the pressure field distribution within the coronary artery. Now for a given coronary artery anatomical model, the pressure field distribution is highly dependent on the outlet boundary condition (BC) in CFD simulation. This is because the BCs are physiologically and mathematically relevant, as the physiological state of the outlet distal vasculature governs its mathematical BC model.<sup>1</sup> Different physiological states correspond to different mathematical models, while a particular outlet BC corresponds to a specific solution of flow pattern and pressure field distribution in the simulated coronary artery.<sup>5</sup> Therefore, in order to accurately determine FFRCT for valid clinical decision-making, the setting of the outlet BC should be patient-specific or personalized, and follow the patient's real physiological state.

However, noninvasively identifying a physiologically personalized (PP)-based outlet BC is highly challenging. This is because it is impractical to noninvasively measure a reliable BC at each outlet, such as flow rate, pressure, or resistance; hence, the outlet BC needs to be set based on patient-specific physiological assumptions.<sup>6</sup> The reliability of the outlet BC is in turn dependent on and limited by the physiological assumption model of coronary blood flow circulation. There is currently no definitive physiological assumption that can accurately quantify patient-specific coronary blood flow and outlet resistance.<sup>7,8</sup> Taylor implemented a method based on the left ventricular mass (LVM) and outlet diameter to estimate and distribute coronary blood flow and outlet resistance.<sup>9</sup> However, the proportional relationship between coronary blood flow and LVM is not constant and varies among individual patients.<sup>10</sup> Hence, this method may not accurately represent the real *in vivo* physiological state for a given patient.

Furthermore, for CFD simulation, we need to segment the coronary vascular geometries of interest, including the major coronary artery with side branches. Limited by the resolution of CTA, the entire coronary artery tree could not be reconstructed, and the small side branches and distal vessels might not be accurately segmented.<sup>11</sup> Therefore, the truncation position of the outlet is critical, as it affects the value of outlet diameter, and hence the distribution of coronary blood flow and the outlet resistance.<sup>12</sup> However, the influence of outlet position truncation strategy on the computed pressure field distribution has not yet been investigated, and there is no guideline regarding the optimal truncation strategy.

So in this study, a PP-based coronary blood flow model is developed for (i) the PP-based outlet BC model by employing the patient-specific quantification of resting coronary blood flow,<sup>25</sup> and (ii) a standardized outlet truncation strategy, to accurately quantify and

distribute coronary blood flow and outlet resistance, for estimating FFRCT. The PP-based BC model quantifies coronary blood flow to be more personalized by introducing additional physiological parameters besides LVM. The standardized truncation strategy can help to optimize the distribution of coronary blood flow and the outlet resistance. These methods adopted in this study will help to improve the accuracy and repeatability of FFRCT estimation, by using invasive FFR as reference.

## 2 | MATERIALS AND METHODOLOGY

In this study, the computational workflow adopted for noninvasive FFRCT estimation is shown in Figure 1, involving several main steps: (a) Loading coronary CTA image data; (b) Segmentation and 3D reconstruction of coronary arteries; (c) Mesh generation; (d) Patient-specific quantification and distribution of resting coronary blood flow and outlet resistance; (e) Reduction of outlet resistance to maximum hyperemia at an adenosine dose of 140 µg/kg/min<sup>13</sup>; (f) CFD calculation to solve the Navier-Stokes equations; (g) Post-processing of patient-specific FFRCT and data analysis.

### 2.1 | Study population

The patients were selected from the "Prospective multicenter clinical trial to evaluate the effectiveness and safety of Hemodyna" study. That study was designed to evaluate the diagnostic accuracy of Hemodyna software (GuanShengYun, Beijing, China) for identifying the hemodynamic significance of coronary stenosis, by using invasive FFR as reference. The study protocol was approved by the ethical review committee of each clinical center, and all patients signed their informed consent. From March 2019 to May 2020, the study recruited a total of 304 patients with suspected coronary artery disease from 5 hospitals in China. Among them, we selected 221 patients for this work. The inclusion criteria were: adult ≥18 years of age, CTA with at least 1 stenosis (site read CT stenosis of 30%-90%) in a major coronary artery ≥2 mm diameter, and undergoing ICA and invasive FFR within 14 days after CTA. The exclusion criteria included prior coronary artery bypass surgery or percutaneous coronary intervention, suspected acute coronary syndrome, recent myocardial infarction within 30 days of CT, and age ≥80 years.

### 2.2 | Medical data acquisition

#### 2.2.1 | Coronary CTA

Coronary CTA was performed by using 64-slice dual-source CT (Siemens SOMATOM Definition Flash,

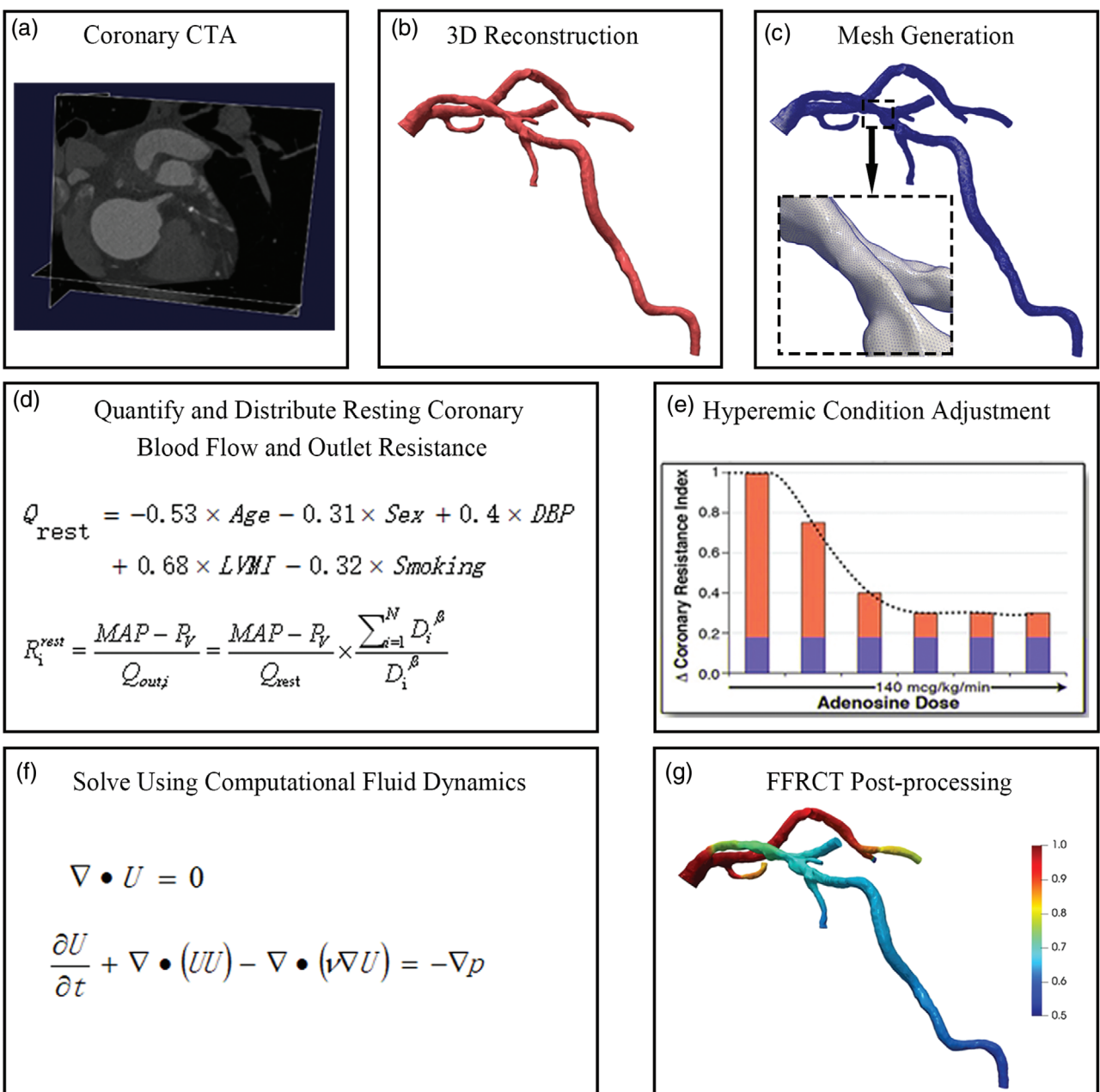


**FIGURE 1** The illustration of noninvasive FFRCT estimation. (a) importing coronary CTA images, (b) coronary artery segmentation and 3D reconstruction, (c) generating the tetrahedral mesh, (d) quantification and distribution of resting coronary blood flow and outlet resistance, (e) adjusting outlet resistance to maximum hyperemia, (f) using computational fluid dynamics to solve the Navier-Stokes equations that govern blood flow, (g) post-processing of patient-specific FFRCT. CTA, computed tomography angiography;  $Q_{rest}$ , total resting coronary blood flow;  $R_i^{rest}$ , resistance at the  $i$ -th outlet; DBP, diastolic blood pressure; LVMI, left ventricular mass index; MAP, mean aortic pressure;  $P_v$ , reference venous pressure;  $Q_{out,i}$ , coronary blood flow at the  $i$ -th outlet;  $D_i$ , average diameter near the  $i$ -th outlet; FFRCT, fractional flow reserve derived from CTA. [Color figure can be viewed at [wileyonlinelibrary.com](http://wileyonlinelibrary.com)]

Erlangen, Germany) or Aquilion ONE 320-slice CT (Toshiba, Tochigi, Japan), according to the Society of cardiovascular computed tomography guidelines.<sup>14</sup> Before scanning, oral beta-blockers were given to patients with a heart rate  $> 75$  bpm. All patients were given nitroglycerin sublingual tablets. During scanning, 80–100 ml of intravenous contrast (Isovue 370 mg/dl)

was injected at 5.0 to 7.0 ml/s, followed by a saline flush. The scanning parameters were: 0.50 to 0.75 mm collimation, tube voltage 100/120 kV, gantry rotation time of 280/300 ms, tube current 300 to 650 mAs, and partial scan. The LVM was measured by using commercial software (Siemens Syngo.via, Erlangen, Germany) for assessment of coronary blood flow.

## 2.2.2 | Invasive coronary angiography and FFR measurement

Invasive coronary angiography (ICA) was performed by catheterization following standard practice within 14 days after coronary CTA.<sup>15</sup> The projection angle was optimized according to the cardiac position, and two projections of each major epicardial vessels were obtained. Invasive FFR was measured based on stenosis severity and lesion characteristics by using Verrata Plus (Philips Volcano, San Diego, USA). Intra-coronary nitroglycerine was given to all patients before insertion of the pressure wire. Hyperemia was induced by continuous intravenous infusion of adenosine at a rate of 140 µg/kg/min. The pressure was measured continuously for several cardiac cycles, and FFR measurements were taken at the lowest observed value. The position of the distal pressure sensor was recorded. Ischemia was defined when the lesion's FFR value was  $\leq 0.80$ .

## 2.2.3 | Clinical data

As part of the clinical routine, the baseline patient characteristics of age, sex, height, weight, blood pressure, heart rate, and smoking history were collected before the ICA examination.

## 2.3 | Coronary artery 3D reconstruction and truncation

In order to reduce the time consumption in CFD simulations, we segmented only the vascular geometries of interest, including the major coronary artery with side branches, and ignored the aorta. Coronary CTA images were segmented by a semi-automatic segmentation algorithm.<sup>19</sup> The segmentation processing steps are illustrated in Figure 2.

To investigate the effect of outlet truncation positions on outlet resistance and FFRCT, we have used two different truncation strategies, as depicted in Figure 3. The Strategy\_1 is a generic method that the side branches be truncated up to the maximum reconstructed branch length. The Strategy\_2 is an optimized standardized strategy of truncation on the straight vascular segment of the first-generation branch of the main coronary, which is approximately five times the branch diameter away from the bifurcation. This strategy avoids the problem of inaccurate segmentation of the distal branch.

## 2.4 | CFD simulation of Navier-Stokes equations, and FFRCT computation

In this study, the blood flow and pressure within the coronary arteries were solved by using the

incompressible Newtonian Navier-Stokes equations given as:

$$\frac{\partial \vec{u}}{\partial t} + (\vec{u} \cdot \nabla) \vec{u} = -\frac{1}{\rho} \nabla p + \nu \nabla^2 \vec{u} \quad (1)$$

$$\nabla \cdot \vec{u} = 0 \quad (2)$$

with  $\vec{u}$  and  $p$  representing the velocity and pressure, and  $t$  the time. The blood is assumed to be an incompressible Newtonian fluid, with dynamic viscosity  $\nu$  of 0.0035 Pa·s and density  $\rho$  of 1050 kg/m<sup>3</sup>. In order to solve the above system of equations, the conditions of domain boundaries should be specified, which is the focus of this study. The vessel wall was assumed to be rigid, with no slip boundary conditions for velocity in all simulations. The vessel wall deformation caused by the motion of cardiac circles was not considered.

The FFRCT value of each point of the artery was calculated by dividing the pressure at that point by the pressure at the ostium of the coronary artery. When comparing the FFRCT with the reference FFR value, the FFRCT value was taken at the site of the pressure sensor (during FFR measurement).

We will now present (i) the Inlet and Outlet BCs, and (ii) quantification and distribution of resting coronary blood flow. This will enable us to define the PP-based outlet BC model and the LVM-based outlet BC model.

## 2.5 | Boundary conditions

The computation of physiologically accurate pressure fields requires appropriate BC to define the blood flow in the vascular network upstream and downstream of the 3D coronary artery geometry. In this study, we have used steady-state BC to compute FFRCT, to reduce computational time and cost. This is based on two reasons. Firstly, the calculation of invasive FFR is based on time-averaged pressure measured over several cardiac cycles. Secondly, it does not matter whether the coronary blood flow rate is supplied uniformly or not, as long as the blood flow meets the myocardial demand for a short time period.

### 2.5.1 | Inlet boundary condition

During the FFR measurement, the mean aortic pressure (MAP) will first increase, and then decrease as the coronary perfusion infuses from resting to hyperemia state. The difference between MAP at the point of FFR measurement and at the resting state is small. Here we ignore this difference and use MAP at resting state as the inlet BC. The MAP can be calculated based on the

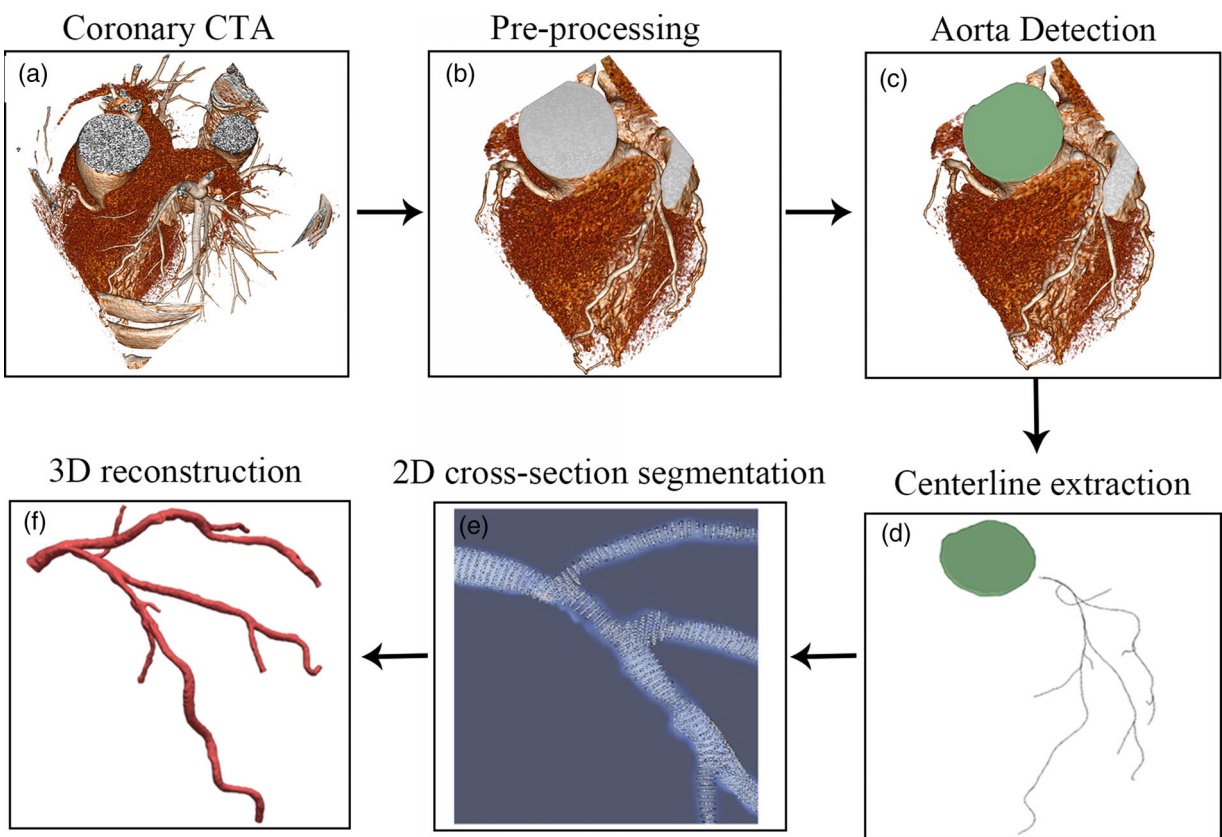


**FIGURE 2** Processing pipeline of coronary artery 3D reconstruction. (a) importing coronary CTA images, (b) pre-processing, such as removing pulmonary vessel, (c) automatically detecting aorta and identifying coronary arteries, (d) extracting coronary centerline and manually setting outlet truncation position, (e) 2D cross-section segmentation, (f) generating 3D coronary surface model. [Color figure can be viewed at wileyonlinelibrary.com]

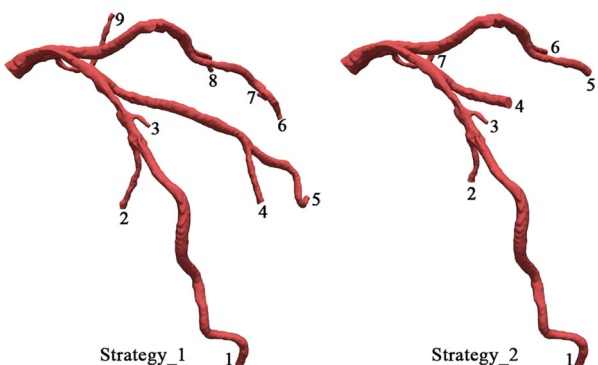


**FIGURE 3** Illustration of outlet truncation strategies. Strategy\_1: truncation up to the maximum reconstructed branch length, Strategy\_2: truncation on the straight vessel segment of the first-generation branches of the main coronary. [Color figure can be viewed at wileyonlinelibrary.com]

brachial cuff-based pressure,<sup>17</sup> as

$$MAP = 0.4 \times (SBP - DBP) + DBP \quad (3)$$

where SBP and DBP are brachial systolic and diastolic blood pressure.

## 2.5.2 | Outlet boundary conditions

When performing the noninvasive FFRCT, we need to simulate the coronary pressure field at hyperemia. This should be especially noted when setting the outlet BCs. The outlet BC models used in this work were assigned by the following procedures to obtain a hyperemic state:

1. Quantify the total resting coronary blood flow ( $Q_{rest}$ ) as explained below in Section 2.F.
2. Allocate blood flow of the left and right coronary branches based on Sakamoto's approach.<sup>18</sup>
3. Distribute coronary blood flow at each outlet according to Murray's law based on the minimum energy hypothesis. The coronary blood flow at the  $i$ -th outlet ( $Q_{out,i}$ ) is expressed as

$$Q_{out,i} = \frac{D_i^\beta}{\sum_{i=1}^N D_i^\beta} \times Q_{rest} \quad (4)$$

where  $D_i$  is the average diameter near the  $i$ -th outlet,  $N$  is the total number of outlets, and  $\beta$  is set to be 2.55.<sup>16</sup>

1. Determine the outlet resistance at the  $i$ -th outlet as

$$R_i^{\text{rest}} = \frac{\text{MAP} - P_v}{Q_{\text{out},i}} \quad (5)$$

where MAP is the mean aortic pressure, and  $P_v$  is a reference venous pressure and set to 5 mmHg.<sup>20</sup> Note that the coronary compliance is ignored in this work as it could not affect the blood pressure field in steady-state simulation.

1. Adjust outlet resistance to maximum hyperemia state, to achieve physiologically accurate computed blood pressure fields.

$$R_i^{\text{hyp}} = R_i^{\text{rest}} \times \text{TCRI} \quad (6)$$

where TCRI is the hyperemia factor and assumed to be 0.16.<sup>13</sup>

## 2.6 | Methods to quantify resting coronary blood flow

The resting coronary blood flow is affected by many factors, including LVM and other patient-specific physiological parameters. The LVM-based method has been the most frequently used in previous noninvasive FFRCT studies. According to allometric scaling law, the LVM-based method assumes the relationship between resting coronary blood flow  $Q_{\text{rest}}$  and LVM as follows:

$$Q_{\text{rest}} = Y_0 \times \text{LVM}^{0.75} \quad (7)$$

where  $Y_0$  is a normalization constant of 0.71,<sup>24</sup> and LVM is acquired by the hospital's CTA workstation.

In order to quantify coronary blood flow more accurately, we have adopted a patient-specific PP-based method in this work. So, in this method,  $Q_{\text{rest}}$  is calculated as<sup>26</sup>:

$$Q_{\text{rest}} = -0.53 \times Y - 0.31 \times G + 0.40 \times \text{DBP} + 0.68 \times \text{LVMI} - 0.32 \times S \quad (8)$$

where (i)  $Y$  (years) is patient's age, (ii)  $G$  (male = 1, female = 0) is patient's sex, (iii) DBP (mmHg) is patient's diastolic blood pressure, (iv)  $S$  (smoking = 1, nonsmoking = 0) is patient's smoking history, and (v) LVMI is left ventricular mass index and calculated as

$$\text{LVMI} = \frac{\text{LVM}}{\text{BSA}} \quad (9)$$

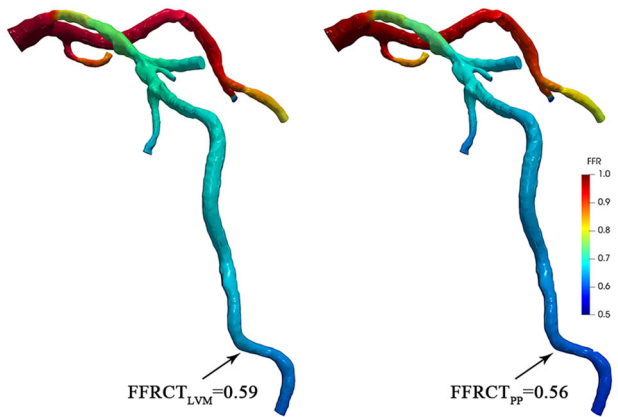


**FIGURE 4** FFRCT computed for a diseased LAD by different outlet BC models, using truncation Strategy\_2. FFRCT<sub>PP</sub>: FFRCT computed by the PP-based outlet BC model; FFRCT<sub>LVM</sub>: FFRCT computed by the LVM-based outlet BC model. [Color figure can be viewed at [wileyonlinelibrary.com](http://wileyonlinelibrary.com)]

$$\text{BSA} = 0.007184 \times W^{0.425} \times H^{0.725} \quad (10)$$

where BSA is the body surface area,<sup>23</sup>  $W$  (kg) and  $H$  (cm) are the patient's weight and height, respectively.

## 2.7 | Defining PP-based outlet BC model and LVM-based outlet BC model

So then (i)  $Q_{\text{rest}}$  given by equation (8), and (ii)  $R_i^{\text{rest}}$  given by equation (5), together define the PP-based outlet BC model.

On the other hand, (i)  $Q_{\text{rest}}$  given by equation (7), and (ii)  $R_i^{\text{rest}}$  given by equation (5), together define the LVM-based outlet BC model.

Then, as indicated in Section 2.D (and also outlined in Figure 1g), the FFRCT value of each point of the artery was computed by dividing the pressure at that point by the pressure at the ostium of the coronary artery. Figure 4 shows the resulting distribution of FFRCT in the coronary tree, by both FFRCT<sub>PP</sub> and FFRCT<sub>LVM</sub>. The color contours provide data on the distribution of FFRCT throughout the coronary tree, and its numerical values can be obtained at any location.

## 2.8 | Statistical analysis

The descriptive variables are presented as mean  $\pm$  SD or as median (quartiles), as appropriate, with categorical variables as percentages. FFR and FFRCT values were recorded on a continuous scale and classified as dichotomous variables with a threshold of 0.80 (values  $\leq 0.80$  considered ischemia). To assess the effect of outlet truncation strategy on FFRCT, a subset of 68 (25%) vessels was randomly selected and

**TABLE 1** Baseline clinical characteristics

Variable	N = 221
Age (years)	61.9±8.0
Men	151(68.3)
Heart rate (bpm)	68.1±5.8
DBP (mmHg)	77.9±10.4
SBP (mmHg)	131.8±17.2
Body surface area ( $m^2$ )	1.69±0.12
Left ventricular mass (g)	143.9±24.4
Hypertension	143(64.7)
Diabetes Mellitus	156(70.6)
Smoker	68(30.8)
Prior Myocardial Infarction	6(2.7)
Prior PCI	10(4.5)
Prior CABG	0(0)
Target Vessels	N = 274
LAD	189(69.0)
LCX	42(15.3)
RCA	43(15.7)
Diameter stenosis level	
30%-50%	19(7)
50%-70%	159(58)
70%-90%	96(35)

Data are presented as mean ± SD or number (%), as appropriate. DBP, diastolic blood pressure; SBP, systolic blood pressure; PCI, percutaneous coronary intervention; CABG, coronary artery bypass surgery; CTA, computed tomography angiography; FFR, fractional flow reserve; LAD, left anterior descending artery; LCX, left circumflex artery; RCA, right coronary artery.

analyzed by two trained operators (S.R and Y.Z). The two operators first performed FFRCT analysis by using truncation strategy\_1, and then using truncation strategy\_2 after one month (as explained in Section 2.3). The operators were blinded to the existing FFRCT and FFR values during FFRCT analysis. The Pearson correlation coefficient, linear regression, Bland-Altman analysis, root-mean-square error (RMSE), concordance correlation coefficient (CCC), and Kappa coefficient were used to assess the inter-operator agreement under the same truncation strategy. Then the FFRCT values calculated by the two operators under the same truncation strategy were averaged to compare the diagnostic performance of the two truncation strategies, including accuracy, sensitivity, specificity, positive predictive value (PPV), and negative predictive value (NPV).

To validate the diagnostic performance of the PP-based outlet BC model, two different BC models (based on resting coronary blood flow,  $Q_{rest}$ ) by using truncation Strategy\_2 were applied to all 274 vessels: i) PP-based BC model, and ii) LVM-based BC model. Using invasive FFR ≤ 0.80 as reference, the diagnostic performances on a per-vessel basis were calculated.

The area under the curve by receiver-operating characteristic analysis (AUC) was also calculated for FFRCT. The relationship between FFRCT and invasive FFR was evaluated by Pearson's correlation coefficients, linear regression, and Bland-Altman analysis. Bias and precision of FFRCT were evaluated by RMSE and CCC. All analyses were performed by MedCalc software (version 15.8, Ostend, Belgium). A two-sided value of  $p < 0.05$  was considered statistically significant.

## 3 | RESULTS

### 3.1 | Baseline clinical and lesion characteristics

A total of 274 vessels from 221 patients were retrospectively enrolled in this study. The baseline patient characteristics are shown in Table 1. The time interval between coronary CTA and invasive FFR was 6.4 ± 4.5 days. The degree of diameter stenosis analysis of coronary CTA was performed by an experienced radiologist in reading cardiac CTA, which resulted in 159 (58%) moderate (50%-70%) stenosis. The average time for FFRCT calculation (from coronary 3D reconstruction to CFD simulation) was about 20 min.

### 3.2 | Validation of the PP-based coronary blood flow model

#### 3.2.1 | Impact of resting coronary blood flow quantification methods on FFRCT<sub>PP</sub> and FFRCT<sub>LVM</sub>

The comparison of total resting coronary blood flow and total outlet resistance of 8 patients with different quantification methods is shown in Table 2. Therein, (i)  $Q_{rest1}$  and  $R_{rest1}$  are the LVM-based method's resting coronary blood flow and total outlet resistance, and (ii)  $Q_{rest2}$  and  $R_{rest2}$  are the PP-based method's resting coronary blood flow and total outlet resistance. For all the enrolled 221 patients,  $Q_{rest1}$  and  $R_{rest1}$  were  $29.4 \pm 3.76$  ml/min and  $3.27 \pm 0.62$  dyn·s/cm<sup>5</sup>, respectively,  $Q_{rest2}$  and  $R_{rest2}$  were  $56.29 \pm 12.70$  ml/min and  $1.76 \pm 0.48$  dyn·s/cm<sup>5</sup>, respectively. The resting coronary blood flow of the PP-based method is approximately twice of the LVM-based method, while the outlet resistance of the PP-based method is about half the LVM-based method.

Then Figure 4 shows the FFRCT values of a case of diseased LAD by the two different quantification methods of resting coronary blood flow, where PP-based FFRCT (FFRCT<sub>PP</sub>) is 0.56, and LVM-based FFRCT (FFRCT<sub>LVM</sub>) is 0.59.

**TABLE 2** Comparison of different resting coronary flow models

No.	Age (years)	Sex (men)	DBP (mmHg)	SBP (mmHg)	BSA (m <sup>2</sup> )	LVM (g)	Smoking history	$Q_{rest1}$ (ml/min)	$Q_{rest2}$ (ml/min)	$10^5 \cdot R_{rest1}$ (dyn*s/cm <sup>5</sup> )	$10^5 \cdot R_{rest2}$ (dyn*s/cm <sup>5</sup> )
1	46	1	80	120	1.83	183	0	35.3	75.2	1.90	0.89
2	63	0	80	130	1.57	130	0	27.3	54.9	2.58	1.29
3	69	0	85	135	1.52	103	0	23.0	43.3	3.20	1.69
4	60	1	65	108	1.90	150	0	30.4	47.4	1.96	1.25
5	58	1	80	120	1.54	118	1	25.4	53.4	2.65	1.26
6	56	1	73	121	1.99	164	1	32.5	55.1	2.02	1.20
7	57	1	80	130	1.84	217	0	40.1	81.8	1.76	0.86
8	66	1	70	120	1.85	125	1	26.5	38.2	2.44	1.69

$Q_{rest1}$  and  $R_{rest1}$  are the LVM-based method's resting coronary blood flow and outlet resistance.  $Q_{rest2}$  and  $R_{rest2}$  are the PP-based method's resting coronary blood flow and outlet resistance. DBP, diastolic blood pressure; SBP, systolic blood pressure; BSA, body surface area; LVM, left ventricular mass.

**TABLE 3** Per-vessel diagnostic performance of FFRCT (N = 274)

	$FFRCT_{PP} \leq 0.80$	$FFRCT_{LVM} \leq 0.80$
Accuracy	91.2(87.3-94.3)	86.5(81.8-90.3)
Sensitivity	90.4(83.0-95.3)	84.6(76.2-90.9)
Specificity	91.8(86.6-95.4)	87.6(81.6-92.1)
PPV	87.0(80.2-91.8)	80.7(73.6-86.3)
NPV	94.0(89.6-96.6)	90.2(85.5-93.6)

Values are proportion in % (95% confidence interval). FFR or FFRCT  $\leq 0.80$  was diagnostic of lesion-specific ischemia.  $FFRCT_{PP}$ , FFRCT computed by the PP-based outlet BC model;  $FFRCT_{LVM}$ , FFRCT computed by the LVM-based outlet BC model; PPV, positive predictive value; NPV, negative predictive value.

### 3.2.2 | Comparing the diagnostic performance of $FFRCT_{PP}$ and $FFRCT_{LVM}$

The vessel-level diagnostic performance of  $FFRCT_{PP}$  and  $FFRCT_{LVM}$  are listed in Table 3, using invasive FFR as reference. As depicted in Figure 5, the AUC of  $FFRCT_{PP}$  and  $FFRCT_{LVM}$  were 0.95 and 0.92, respectively. The scatterplots and Bland-Altman plots for  $FFRCT_{PP}$  and  $FFRCT_{LVM}$  are shown in Figure 6, in relation to invasive FFR. Therein,  $FFRCT_{PP}$  and  $FFRCT_{LVM}$  demonstrated Pearson correlation of 0.875 and 0.789, limits of agreement of -0.09 to 0.09, and -0.11 to 0.12, respectively. In addition, the RMSE and CCC of  $FFRCT_{PP}$  were 0.047 and 0.874 (0.843-0.899), respectively, and 0.060 and 0.785 (0.736-0.826) of  $FFRCT_{LVM}$ , respectively.

### 3.3 | Diagnostic performance of $FFRCT_{PP}$ and $FFRCT_{LVM}$ in moderate coronary stenosis

Among the 159 vessels with moderate (50% to 70%) stenosis on coronary CTA images, 51 (30.5%) vessels exhibited an ischemia FFR value of  $\leq 0.80$ . For

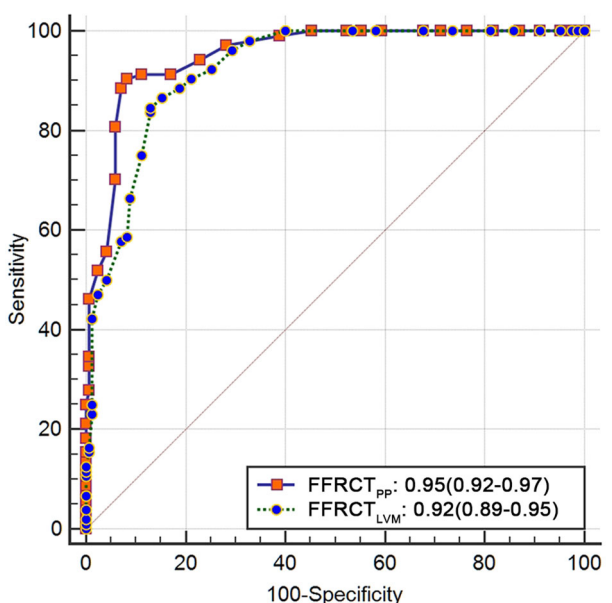


**FIGURE 5** Comparison of receiver-operating curves for  $FFRCT_{PP}$  and  $FFRCT_{LVM}$ . Results presented as area under curves (95% confidence interval).  $FFRCT_{PP}$ : FFRCT computed by the PP-based outlet BC model;  $FFRCT_{LVM}$ : FFRCT computed by the LVM-based outlet BC model. [Color figure can be viewed at wileyonlinelibrary.com]

these vessels, by using invasive FFR as reference, the diagnostic performance of  $FFRCT_{PP}$  and  $FFRCT_{LVM}$  are listed in Table 4. As depicted in Figure 7, the AUC of  $FFRCT_{PP}$  and  $FFRCT_{LVM}$  were 0.92 and 0.90, respectively. Figure 8 shows the scatterplots and Bland-Altman plots for  $FFRCT_{PP}$  and  $FFRCT_{LVM}$ , showing their correlation and agreement with invasive FFR, in the subgroup of moderate stenosis vessels. In addition, the RMSE and CCC of (i)  $FFRCT_{PP}$  were 0.049 and 0.799 (0.735-0.849), respectively, and (ii) 0.060 and 0.707 (0.620-0.777) of  $FFRCT_{LVM}$ , respectively.

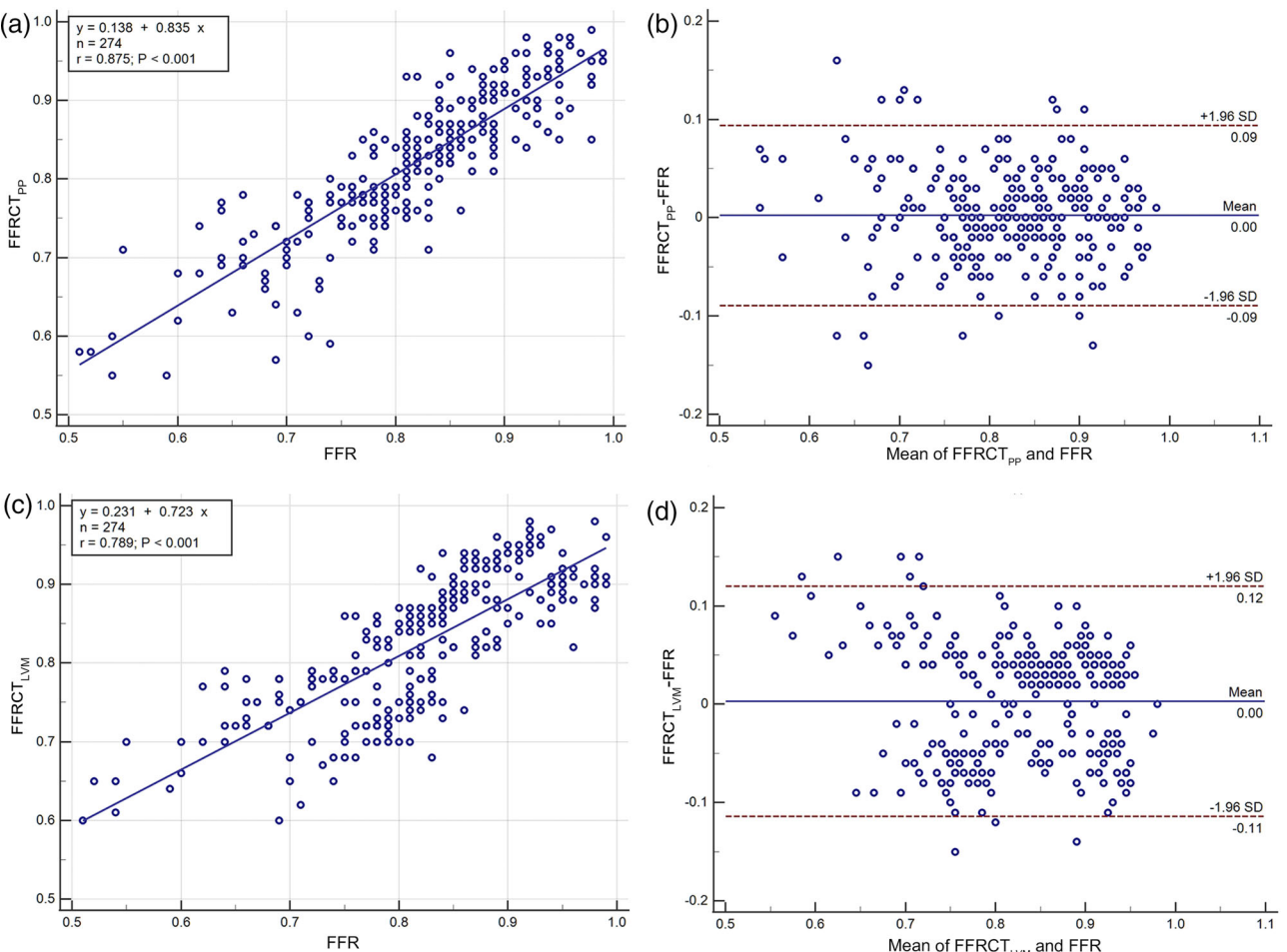


**FIGURE 6** Correlation and agreement between FFR and FFRCT. FFRCT<sub>PP</sub>: FFRCT computed by the PP-based outlet BC model; FFRCT<sub>LVM</sub>: FFRCT computed by the LVM-based outlet BC model. [Color figure can be viewed at [wileyonlinelibrary.com](http://wileyonlinelibrary.com)]

**TABLE 4** Per-vessel diagnostic performance of FFRCT in moderate stenosis ( $N = 159$ )

	FFRCT <sub>PP</sub> ≤ 0.80	FFRCT <sub>LVM</sub> ≤ 0.80
Accuracy	88.7(82.7-93.2)	82.4(75.6-88.0)
Sensitivity	82.4(65.5-93.2)	76.5(58.8-89.3)
Specificity	90.4(83.8-94.9)	84.0(76.4-89.9)
PPV	70.0(57.1-80.3)	56.5(45.5-66.9)
NPV	94.9(90.1-97.5)	92.9(87.7-96.0)

Values are proportion in % (95% confidence interval). FFR or FFRCT  $\leq 0.80$  was diagnostic of lesion-specific ischemia. FFRCT<sub>PP</sub>: FFRCT computed by the PP-based outlet BC model; FFRCT<sub>LVM</sub>: FFRCT computed by the LVM-based outlet BC model; PPV, positive predictive value; NPV, negative predictive value.

### 3.4 | Impact of outlet truncation position on FFRCT

Table 5 shows the outlet diameter and resting resistance at each outlet for a patient's left coronary artery with different outlet truncation strategies. For all the 68 vessels, the outlet diameter and resistance of (i) Strategy\_1 were  $1.75 \pm 0.45$  mm and  $16.88 \pm 6.61$  dyn·s/cm<sup>5</sup>, respectively, and (ii)  $1.93 \pm 0.41$  mm and  $14.45 \pm$

**TABLE 5** Impact of outlet truncation position on outlet resistances

Outlets No.	D1(mm)	D2(mm)	$10^5 \times R1$ (dyn·s/cm <sup>5</sup> )	$10^5 \times R2$ (dyn·s/cm <sup>5</sup> )
1	1.82	1.82	6.18	8.00
2	1.23	1.41	16.78	15.35
3	1.00	1.00	28.45	36.85
4	1.48	2.18	10.47	5.05
5	1.17	1.97	19.06	6.54
6	1.50	1.51	10.12	12.89
7	1.36	1.52	12.99	12.67
8	1.35	—	13.23	—
9	1.30	—	14.57	—

D1 and R1 are the outlet diameter and resistance at the i-th outlet with truncation on the straight vessel segment of the first-generation branch of the main coronary; D2 and R2 are the outlet diameter and resistance at the i-th outlet with truncation up to the maximum reconstructed branch length.

6.25 dyn·s/cm<sup>5</sup> of Strategy\_2, respectively. The FFRCT values based on the PP-based outlet BC model under these two truncation strategies are shown in Figure 9.

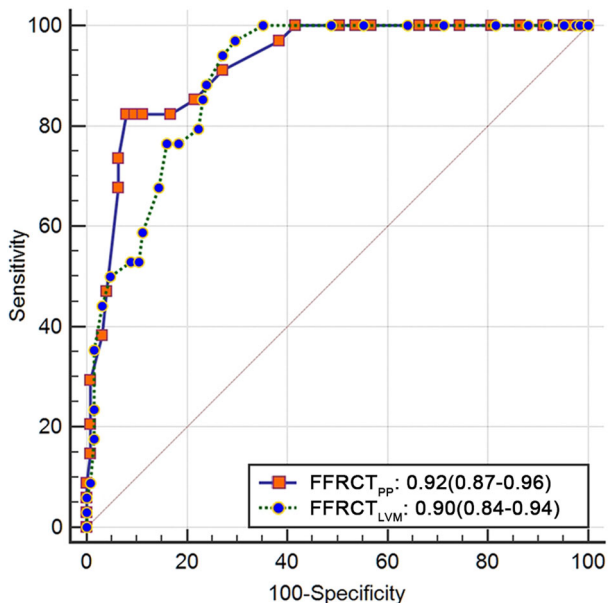


**FIGURE 7** Comparison of receiver-operating curves for FFRCT in subgroup of moderate stenosis vessels. Results presented as area under curves (95% confidence interval). FFRCT<sub>PP</sub>: FFRCT computed by the PP-based outlet BC model; FFRCT<sub>LVM</sub>: FFRCT computed by the LVM-based outlet BC model. [Color figure can be viewed at wileyonlinelibrary.com]

Considering FFRCT as continuous variable, the scatterplots and Bland-Altman plots between operators for Strategy\_1 and Strategy\_2 are shown in Figure 10. In addition, the CCC of Strategy\_1 and Strategy\_2 were 0.816 (0.718-0.882) and 0.927 (0.884-0.954), respectively. Using FFRCT  $\leq 0.80$  as the cut-off value, the Kappa coefficient values of Strategy\_1 and Strategy\_2 were 0.907 (0.805-1.00) and 0.908 (0.807-1.00), respectively. Besides, the truncation Strategy\_1 and Strategy\_2 had accuracy of 83.3% (72.1%-91.4%) versus 89.7% (79.9%-95.8%), sensitivity of 77.8% (57.7%-91.4%) versus 86.2% (68.3%-96.1%), specificity of 87.2% (72.5%-95.7%) versus 92.3% (79.3%-98.4%), PPV of 80.8% (64.4%-90.7%) versus 89.2% (73.6%-96.2%), and NPV of 85.0% (73.5%-92.1%) vs 90.2% (78.3%-95.7%).

## 4 | DISCUSSION

In this study, we have developed a PP-based coronary blood flow model, involving (i) a PP-based outlet BC model based on employing the patient-specific quantification of resting coronary blood flow, and (ii) a standardized outlet truncation strategy to improve the capability of FFRCT estimation. When estimating the resting coronary blood flow, the PP-based model involved more physiological parameters of the patient besides LVM, as shown in Equation (8). The results, as displayed in Tables 3 and 4 showed that compared with the LVM-based model, the PP-based model could

improve FFRCT diagnostic performance, especially for vessels with moderate stenosis. We also investigated the impact of outlet truncation position on FFRCT estimation, and found that the standardized truncation strategy could improve the repeatability of FFRCT.

The value of FFRCT is influenced by the coronary outlet resistance.<sup>21</sup> The equivalent circuit model of coronary blood circulation, as presented by Prijis, shows that the stenotic coronary resistance ( $R_{\text{sten}}$ ) and distal microvascular resistance ( $R_{\text{cmvc}}$ ) are actually two resistors connected in series.<sup>22,26</sup> Now the clinical definition of FFR is the ratio of the stenotic distal mean pressure to the proximal mean pressure, which is equivalent to  $R_{\text{cmvc}}/(R_{\text{sten}} + R_{\text{cmvc}})$ . Therefore, the value of FFRCT completely depends on the parameters of  $R_{\text{sten}}$  and  $R_{\text{cmvc}}$ . The  $R_{\text{sten}}$  is determined by the 3D model of stenotic coronary arteries and is influenced by the segmentation accuracy, which is not considered in this study. The  $R_{\text{cmvc}}$  is the outlet resistance and determined by the outlet resistance assessment method.

The resting coronary blood flow affects the total coronary outlet resistance.<sup>9</sup> It is hence an essential parameter in the calculation of total coronary outlet resistance. Since it is impossible to directly obtain the resistance of each coronary outlet, we need to apply physiological assumption based on existing data to make a reasonable estimation. Muller has investigated the influence of several methods available in the literature to estimate resting coronary blood flow on FFRCT estimation.<sup>20</sup> That study has shown that the resting coronary blood flow estimating method does have a significant impact on the diagnostic performance of FFRCT. However, these current methods cannot significantly improve the estimation error standard deviation.

The PP-based method for resting coronary blood flow, according to Reference<sup>25</sup>, could improve the accuracy of estimating patient-specific resting coronary blood flow. First, the measurement of coronary blood flow in Reference<sup>25</sup> should be reliable, as it was measured through a Doppler-tipped guidewire advancing into the proximal portion of the patient's coronary artery. In principle, Doppler guidewire can directly measure the velocity of blood cells. Changes in red blood cell velocity result in corresponding Doppler frequency shift, which allows quantification of absolute velocities and instantaneous detection of changes in these velocities.<sup>27</sup> In vitro and in vivo studies have both demonstrated high accuracy of the Doppler guidewire for measuring coronary blood flow.<sup>28,29</sup> While in Reference<sup>24</sup>, the coronary blood flow was measured based on an isolated swine heart by perfusing with a cardioplegic solution into the coronary arteries down to the precapillary level. The coronary blood flow measurement was not under the actual physiological state. We think this may be the reason why  $Q_{\text{rest2}}$  assessed by the PP-based method is higher than  $Q_{\text{rest1}}$  by the LVM-based method in Table 2. Second, this PP-based method has incorporated

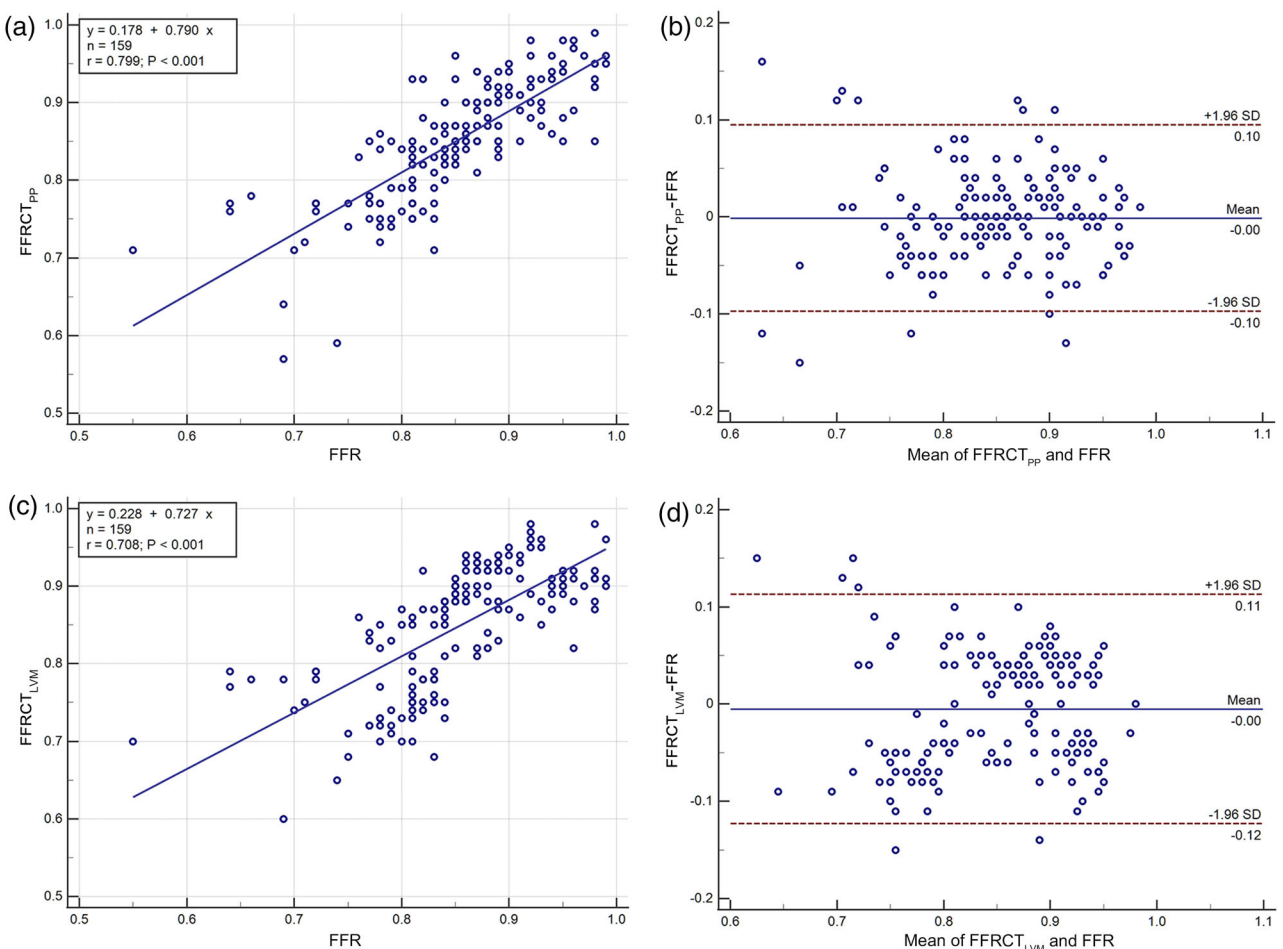


**FIGURE 8** Correlation and agreement between FFR and FFRCT in the subgroup of moderate stenosis vessels. FFRCT<sub>PP</sub>: FFRCT computed by the PP-based outlet BC model; FFRCT<sub>LVM</sub>: FFRCT computed by the LVM-based outlet BC model. [Color figure can be viewed at wileyonlinelibrary.com]

several patient parameters and followed the cardiovascular physiological basis. Among these parameters, LVMI, DBP, and age are the ones that have the greatest impact on resting coronary blood flow. It is known that resting coronary blood flow is mainly determined by the myocardial demand.<sup>30</sup> The LVMI determines the fundamental myocardial demand and provides the base value of resting coronary blood flow, while DBP and age together regulate the patient-specific variations in coronary blood flow. The increase in DBP leads to an increase in resting coronary blood flow, as coronary blood flow is driven by DBP, while left ventricular load and myocardial demand increase with DBP.<sup>31,32</sup> This is consistent with Equation 8 in this work. When DBP was excluded from Equation 8, the term of 0.40\*DBP was deleted. The  $Q_{rest}$  without DBP was about 31 ml/min smaller than  $Q_{rest}$  with DBP, since the average DBP of patients was 77.9 mmHg (as seen in Table 1). In addition, for the middle-aged to elderly population, metabolic and myocardial demand will gradually decrease with age, and thus resting coronary blood flow decreases

with age.<sup>33</sup> Third, we have validated the diagnostic performance of FFRCT calculated by our PP-based method using a dataset of 274 vessels.

Our PP-based coronary blood flow model involves (i) a patient-specific PP-based outlet BC model based on employing the patient-specific quantification of resting coronary blood flow,<sup>25</sup> and (ii) a standardized outlet truncation strategy to improve the capability of FFRCT estimation. As shown in Tables 3 and 4, by using invasive FFR as reference, the diagnostic performance of FFRCT<sub>PP</sub> was better than that of FFRCT<sub>LVM</sub>. The reason may be that the assessment of coronary blood flow and outlet resistance by the PP-based method is closer to the patient's physiological condition. It can be seen from Table 2 that there is a large difference in the resting coronary blood flow assessed by these two methods. Among the eight randomly selected patients, the value of  $Q_{rest1}$  was generally lower than  $Q_{rest2}$ , while  $R_{t,rest1}$  was higher than  $R_{t,rest2}$ .

The outlet diameter affects the coronary blood flow distribution among the outlets, and the values of outlet

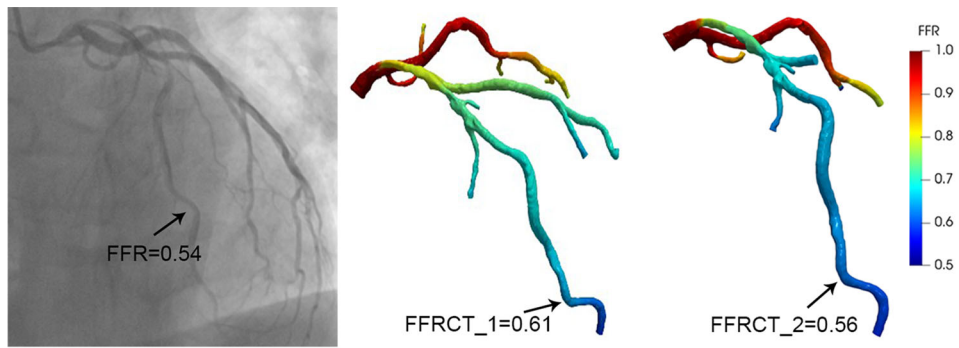


**FIGURE 9** Distribution of FFRCT computed based on the PP-based outlet BC model under different truncation strategies. FFRCT<sub>1</sub> was calculated by the truncation Strategy<sub>1</sub>; FFRCT<sub>2</sub> was calculated by the truncation Strategy<sub>2</sub>. [Color figure can be viewed at [wileyonlinelibrary.com](http://wileyonlinelibrary.com)]

resistance. Hence, a reasonable outlet truncation strategy helps to improve the repeatability of FFRCT. Since the diameters of the coronary vessel are not uniform, the size of the outlet diameter is affected by the outlet truncation position. However, there is currently no consensus on where the coronary outlet should be truncated. According to the SCCTA guidelines, clinicians usually only pay attention to stenosis in vessels up to 2 mm in diameter.<sup>14</sup> Besides, the segmentation of small side branches and distal vessels might not be sufficiently accurate, due to the relatively low resolution of CTA and dissipation of contrast agents along the vessel.<sup>11</sup> According to Murray's law, the outlet diameter is related to the blood flow distribution between branches.<sup>12</sup> Therefore, if the outlet diameter of the extracted side branch is smaller than the actual diameter of the vessel, a lower blood flow will be allocated and the blood flow rate in the side branch will be lower than the actual flow rate. Then in turn, the lower blood flow rate will produce a lower pressure drop along with the stenosis, thereby affecting the value of FFR. In this regard, Uus has presented a truncation strategy that the side branches should be truncated at a certain level of the lumen diameter, such as 2 mm.<sup>34</sup> That study has found differences in FFR between this truncation strategy and the conventional truncation strategy that truncated up to the maximum reconstructed branch length. However, it did not further investigate the effect of outlet truncation position on the diagnostic performance of FFRCT. Therefore, in this study, we have developed and carried out a standardized truncation strategy that truncates on a straight segment of the first-generation branches of the main coronary artery. This strategy avoids the problem of inaccurate segmentation of the distal branch coronary. As shown in Figure 10, this strategy has better repeatability and slightly higher diagnostic accuracy than the conventional truncation strategy.

For FFRCT calculation, the CFD model assumptions, such as Newtonian fluid and rigid wall, need to be included. Sankaran et al. investigated the uncertainty

quantification in FFRCT calculation and found that the impact of blood viscosity was less than 3D reconstruction and outlet boundary resistance.<sup>35</sup> Gashi evaluated the effect of blood viscosity on the calculated FFRCT by considering blood as a Newtonian fluid with fixed viscosity or a non-Newtonian fluid with varying viscosities.<sup>36</sup> The results showed that for invasive FFR between 0.70 and 0.80 (the critical range of FFR), the viscosity model should be selected carefully to reduce the uncertainty in FFRCT calculation. So in future studies, personalized and accurate blood viscosity models should be used instead of fixed viscosity based on the population average to improve the accuracy of FFRCT. In addition, the wall deformation caused by the periodic cardiac motion would affect the blood flow field. Seo et al. and Xu et al. evaluated the impact of elastic wall deformation on the calculated FFRCT of coronary and carotid arteries, respectively.<sup>37,38</sup> Both studies have found that the FFRCT values calculated under different elastic modulus were almost identical. It is because the wall deformation only affects the blood pressure waveform, but not the average pressure, which is used for FFR/FFRCT definition. Therefore, the rigid wall is appropriate for FFRCT calculation.

Nevertheless, the present study has some limitations. First, the resting coronary blood flow may still not be evaluated accurately in patients with pathological conditions, such as those with microvascular disease, despite the addition of some patient-specific physiological parameters to the modeling assumption. It is possible to improve the model by including other parameters, such as diabetes status.<sup>38</sup> Second, this study did not consider the impact of patient-specific hyperemia factor TCRI on the diagnostic accuracy of FFRCT. For patients with microvascular disease, the adenosine-mediated hyperemia model may overestimate the degree of vasodilation, resulting in lower FFRCT values than invasive FFR measurements. However, as far as we know, there is no non-invasive, drug-free, or additional imaging method to assess TCRI. Third, the FFRCT computational

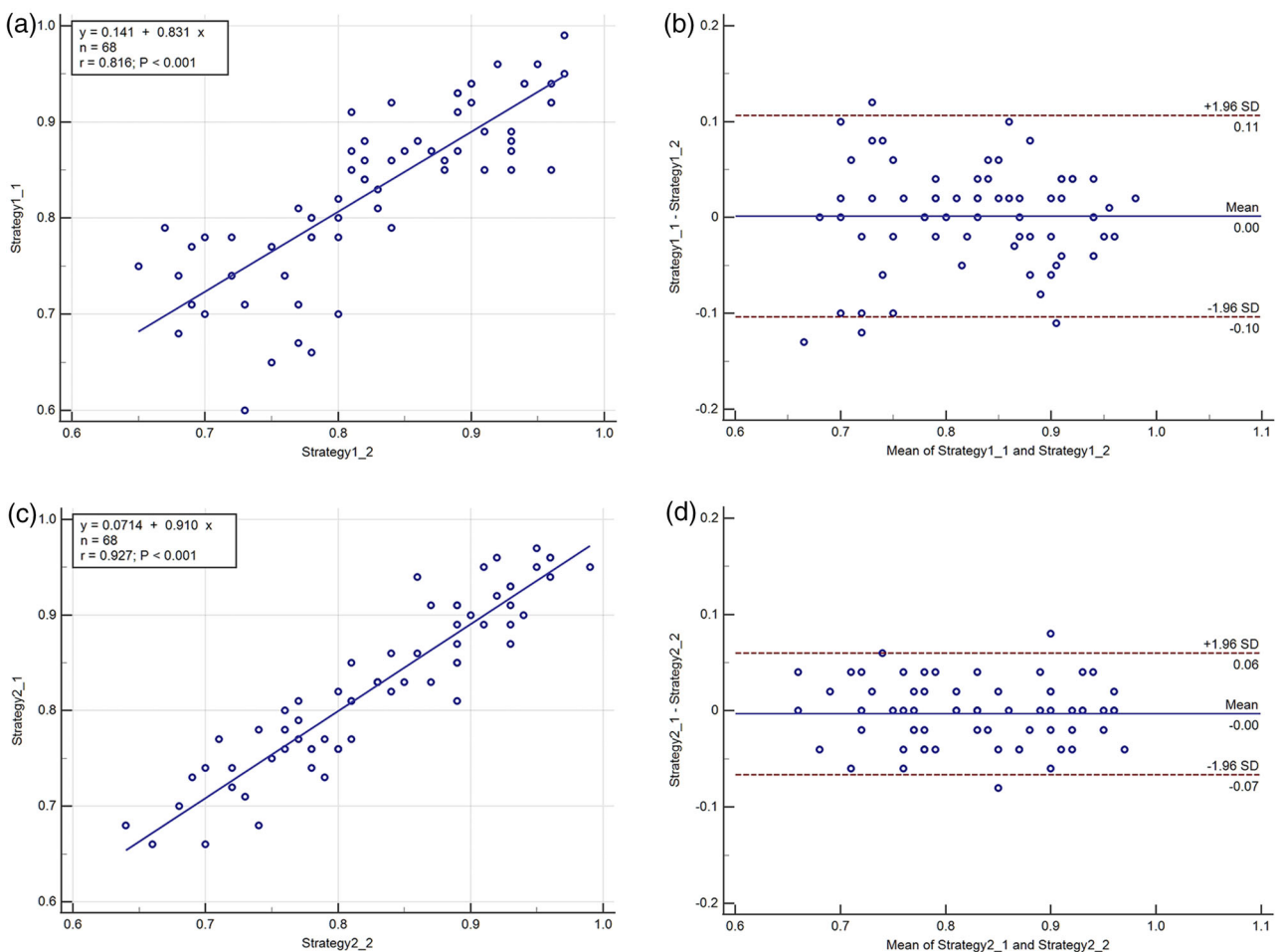


**FIGURE 10** Correlation and agreement demonstrating repeatability of FFRCT analysis of outlet truncation strategies. Strategy1\_1 and Strategy1\_2: FFRCT calculated (using the PP-based outlet BC model) based on truncation Strategy\_1 by two operators; Strategy2\_1 and Strategy2\_2: FFRCT calculated (using the PP-based outlet BC model) based on truncation Strategy\_2 by two operators. [Color figure can be viewed at [wileyonlinelibrary.com](http://wileyonlinelibrary.com)]

procedure in this study was not a fully automated process. Although we have proposed a standardized outlet truncation strategy, the modeling process still requires manual interaction processing by the operator. Hence, the repeatability of FFRCT is somewhat affected by the operator's experience. Fourth, although the PP-based resting coronary blood flow model was reliable, the model remains limited due to the small study size in Reference<sup>25</sup>. If the model had been validated in a much larger number of subjects, the coefficients from the model fit would be different, which could change the result of this study. Fifth, this study used only a subset rather than the entire dataset to verify the feasibility of the standardized truncation strategy, since the results could change by using the entire dataset. Finally, similar to other FFRCT assessment methods, our method also relies on accurate segmentation of coronary arteries. This remains a challenging work limited by CTA image resolution and potential imaging artifacts.

## 5 | CONCLUSIONS

This study has demonstrated that our PP-based coronary blood flow model, involving (i) the PP-based outlet BC by employing the patient-specific quantification of resting coronary blood flow, and (ii) the standardized outlet truncation strategy can together improve the capability to better estimate FFRCT. The PP-based model introduces additional physiological parameters other than LVM to quantify coronary blood flow and assess the outlet resistance. The analysis of 274 vessels has shown that this integrated PP-based model improves the diagnostic performance of FFRCT, in relation to invasive FFR as reference. In addition, it is seen that the standardized truncation strategy improves also FFRCT repeatability.

## ACKNOWLEDGMENTS

This work was supported by the Key-Area Research and Development Program of Guangdong Province (2019B010110001), the National Natural Science

Foundation of China (62101610, 62101606), the China Postdoctoral Science Foundation (2021M693673), the Shenzhen Science and Techonlogy Program (2021A14), the British Heart Foundation (TG/18/5/34111, PG/16/78/32402), the European Research Council Innovative Medicines Initiative (DRAGON, H2020-JTI-IMI2 101005122), the AI for Health Imaging Award (CHAIMELEON, H2020-SC1-FA-DTS-2019-1 952172), and the UK Research and Innovation Future Leaders Fellowship (MR/V023799/1). The authors gratefully acknowledge Dr. Lin Yang, a radiologist experienced in reading cardiac CT from Beijing Anzhen Hospital.

## CONFLICT OF INTEREST

The authors have no relevant conflict of interest to disclose. The concepts and information presented in this work are based on research, and the work was not biased due to any commercial influence.

## DATA AVAILABILITY STATEMENT

Research data are not shared.

## REFERENCES

- Min JK, Taylor CA, Achenbach S, et al. Noninvasive fractional flow reserve derived from coronary CT angiography: clinical data and scientific principles. *JACC Cardiovasc Imaging*. 2015;8(10):1209-1222.
- Tesche C, De Cecco CN, Albrecht MH, et al. Coronary CT angiography-derived fractional flow reserve. *Radiology*. 2017;285(1):17-33.
- Liu X, Mo X, Yang G, Shi C, Hau WK. A 2-year investigation of the impact of the computed tomography-derived fractional flow reserve calculated using a deep learning algorithm on routine decision-making for coronary artery disease management. *Eur Radiol*. 2021;1:8.
- Fairbairn TA, Nieman K, Akasaka T, et al. Real-world clinical utility and impact on clinical decision-making of coronary computed tomography angiography-derived fractional flow reserve: lessons from the ADVANCE Registry. *Eur Heart J*. 2018;39(41):3701-3711.
- Feiger B, Vardhan M, Gounley J, et al. Suitability of lattice Boltzmann inlet and outlet boundary conditions for simulating flow in image-derived vasculature. *Int J Numer Method Biomed Eng*. 2019;35(6):e3198.
- Morris PD, van de Vosse FN, Lawford PV, Hose DR, Gunn JP. Virtual"(computed) fractional flow reserve: current challenges and limitations. *JACC Cardiovasc Interv*. 2015;8(8):1009-1017.
- Feher A, Sinusas AJ. Quantitative assessment of coronary microvascular function: dynamic single-photon emission computed tomography, positron emission tomography, ultrasound, computed tomography, and magnetic resonance imaging. *Circ Cardiovasc Imaging*. 2017;10(8):e006427.
- Camici PG, d'Amati G, Rimoldi O. Coronary microvascular dysfunction: mechanisms and functional assessment. *Nat Rev Cardiol*. 2015;12(1):48-62.
- Taylor CA, Fonte TA, Min JK. Computational fluid dynamics applied to cardiac computed tomography for noninvasive quantification of fractional flow reserve: scientific basis. *J Am Coll Cardiol*. 2013;61(22):2233-2241.
- Rabkin S. Considerations in Understanding the Coronary Blood Flow- Left Ventricular Mass Relationship in Patients with Hypertension. *Curr. Cardiol. Rev.* 2016;13(1):75-83. <http://doi.org/10.2174/157339711266160909093642>
- De Feyter PJ, Krestin GG, Cademartiri F, et al. *Computed tomography of the coronary arteries*. CRC Press; 2008. <https://doi.org/10.3109/9780203091654>
- Murray CD. The physiological principle of minimum work applied to the angle of branching of arteries. *J Gen Physiol*. 1926;9(6):835-841.
- Wilson RF, Wyche K, Christensen BV, Zimmer S, Laxson DD. Effects of adenosine on human coronary arterial circulation. *Circulation*. 1990;82(5):1595-1606.
- Abbara S, Arbab-Zadeh A, Callister TQ, et al. SCCT guidelines for performance of coronary computed tomographic angiography: a report of the Society of Cardiovascular Computed Tomography Guidelines Committee. *J Cardiovasc Comput Tomogr*. 2009;3(3):190-204.
- Naidu SS, Rao SV, Blankenship J, et al. Clinical expert consensus statement on best practices in the cardiac catheterization laboratory: society for Cardiovascular Angiography and Interventions. *Catheter Cardiovasc Interv*. 2012;80(3):456-464.
- Schwarz JCV, van Lier MGJTB, van den Wijngaard JPHM, Siebes M, VanBavel E. Topologic and Hemodynamic Characteristics of the Human Coronary Arterial Circulation. *Front Physiol*. 2020;10:1611.
- Bos WJ, Verrij E, Vincent HH, Westerhof BE, Parati G, van Montfrans GA. How to assess mean blood pressure properly at the brachial artery level. *J Hypertens*. 2007;25(4):751-755.
- Sakamoto S, Takahashi S, Coskun AU, et al. Relation of distribution of coronary blood flow volume to coronary artery dominance. *Am J cardiol*. 2013;111(10):1420-1424.
- Yang G, Kitslaar P, Frenay M, et al. Automatic centerline extraction of coronary arteries in coronary computed tomographic angiography. *Int J Cardiovas Imag*. 2012;28(4):921-933.
- Müller LO, Fossan FE, Bråten AT, et al. Impact of baseline coronary flow and its distribution on fractional flow reserve prediction. *Int. J. Numer. Methods Biomed. Eng.* 2021;37(11), <http://doi.org/10.1002/cnm.3246>
- Sommer KN, Shepard LM, Mitsouras D, et al. Patient-specific 3D-printed coronary models based on coronary computed tomography angiography volumes to investigate flow conditions in coronary artery disease. *Biomed Phys Eng Expr*. 2020;6(4):045007.
- Faes TJ, Meer R, Heyndrickx GR, Kerkhof P. Fractional Flow Reserve Evaluated as Metric of Coronary Stenosis|A Mathematical Model Study. *Front Cardiovasc Med*. 2020(6):189.
- Du Bois D, Du Bois E. A formula to estimate the approximate surface area if height and weight be known. *Nutrition*. 1989;5(5):303-313.
- Choy JS, Kassab GS. Scaling of myocardial mass to flow and morphometry of coronary arteries. *J Appl Physiol*. 2008;104(5): 1281-1286.
- Misawa K, Nitta Y, Matsubara T, et al. Difference in coronary blood flow dynamics between patients with hypertension and those with hypertrophic cardiomyopathy. *Hypertens Res*. 2002;25(5):711-716.
- Pijls N, De Bruyne B. Coronary pressure measurement and fractional flow reserve. *Heart*. 1998;80(6):539-542.
- Wilson RF, Laughlin D, Ackell PH, et al. Transluminal, subselective measurement of coronary artery blood flow velocity and vasodilator reserve in man. *Circulation*. 1985;72(1):82-92.
- Labovitz AJ, Anthonis DM, Cravens TL, Kern MJ. Validation of volumetric flow measurements by means of a Doppler-tipped coronary angioplasty guide wire. *Am Heart J*. 1993;126(6):1456-1461.
- Doucette JW, Corl PD, Payne HM, et al. Validation of a Doppler guide wire for intravascular measurement of coronary artery flow velocity. *Circulation*. 1992;85(5):1899-1911. <http://doi.org/10.1161/01.cir.85.5.1899>

30. Wieneke H, Von Birgelen C, Haude M, et al. Determinants of coronary blood flow in humans: quantification by intracoronary Doppler and ultrasound. *J Appl Physiol.* 2005;98(3):1076-1082.
31. Rabkin SW, Shiekh IA, Wood DA. The impact of left ventricular mass on diastolic blood pressure targets for patients with coronary artery disease. *Am J Hypertens.* 2016;29(9):1085-1093.
32. Feigl EO, Neat GW, Huang AH. Interrelations between coronary artery pressure, myocardial metabolism and coronary blood flow. *J Mol Cell Cardiol.* 1990;22(4):375-390.
33. Yaniv Y, Juhaszova M, Sollott SJ. Age-related changes of myocardial ATP supply and demand mechanisms. *Trends in Endocrinol Metab.* 2013;24(10):495-505.
34. Uus A. *Patient-specific blood flow modelling in diagnosis of coronary artery disease.* City University London; 2016.
35. Sankaran S, Kim HJ, Choi G, Taylor CA. Uncertainty quantification in coronary blood flow simulations: impact of geometry, boundary conditions and blood viscosity. *J Biomech.* 2016;49(12):2540-2547.
36. Gashi K. The impact of model assumptions on coronary blood flow computations. PhD thesis, Eindhoven university of technology. 2019.
37. Seo J, Schiavazzi DE, Kahn AM, Marsden AL. The effects of clinically-derived parametric data uncertainty in patient-specific coronary simulations with deformable walls. *Int J Numer Meth Bio.* 2020;36(8):e3351.
38. Xu K, Yu L, Wan J, Wang S, Lu H. The influence of the elastic modulus of the plaque in carotid artery on the computed results of FFRCT. *Comput Method Biomed.* 2020;23(5):201-211.
39. Lembo M, Sicari R, Esposito R, et al. Association between elevated pulse pressure and high resting coronary blood flow velocity in patients with angiographically normal epicardial coronary arteries. *J Am Heart Assoc.* 2017;6(7):e005710.

**How to cite this article:** Liu X, Xu C, Rao S, et al. Physiologically personalized coronary blood flow model to improve the estimation of noninvasive fractional flow reserve. *Med Phys.* 2022;49:583–597.  
<https://doi.org/10.1002/mp.15363>